Raman scattering in single crystal C_{60}

P.H.M. van Loosdrecht [a], P.J.M. van Bentum [a,b], M.A. Verheijen [a] and G. Meijer [a]

[a] *Research Institute of Materials, University of Nijmegen, Toernooiveld, 6525 ED Nijmegen, The Netherlands*

[b] *IBM Thomas J. Watson Research Center, Yorktown Heights, NY 10598, USA*

Received 24 June 1992; in final form 17 August 1992

Raman spectra (using 514 and 740 nm excitation) of high-purity single crystal C_{60} are presented for the high- and low-temperature phases, showing activity of all "gerade" modes. Within the experimental accuracy, the spectra are found to be consistent with the selection rules for Raman scattering in both the high-temperature fcc and low-temperature $2a_0$-fcc phases of solid C_{60}. A complete assignment of the observed peaks is proposed.

1. Introduction

The discovery of buckminsterfullerene [1] (C_{60}), and in particular the development of a method [2] to produce macroscopic quantities of the fullerenes, has launched a enormous research effort to characterize and understand the chemical and physical properties of this exciting new form of carbon as well as of its derivatives [3] [#1]. Recently, the solid-state properties of the fullerenes have gained much interest, partly induced by the discovery of "high-temperature" superconductivity in alkali-intercalated C_{60} [4] and by the unusual dynamics of the nearly spherical C_{60} molecules in the crystal lattice [5–7]. Crystalline C_{60} is a molecular solid with only weak intermolecular forces. Despite the weak lattice interactions the presence of the crystal field has a distinct influence on the properties of solid C_{60}. A clear example of this is the phase transition at $T \approx 255$ K, involving a critical decrease of the quasi-free rotational motions. Other manifestations of solid-state effects are for instance found in changes of the resonant enhancements of inelastic light scattering processes [8] and the presence of several species of delocalized excitons [9] in solid C_{60}.

Raman spectroscopy has proved to be a convenient method to study the solid-state effects on the dynamical properties of C_{60} and related compounds. It has been shown recently that the reduction of the high I_h symmetry of the free molecule in the crystal lattice leads to splittings of molecular degenerate vibrational modes and to activation of modes which are Raman inactive for the free molecule. Also a coupling of the vibrational modes to the rotational excitations of C_{60} [10], and to the electronic excitations in alkali-intercalated C_{60} [11] have been reported.

The present Letter presents a detailed Raman spectroscopic study of the solid-state vibrational properties of single crystal C_{60} in the high-temperature fcc and the low-temperature $2a_0$-fcc phases [12]. A full assignment of the observed peaks is proposed, deduced from the selection rules and a comparison of the data presented here to other experimental data [2,13] and to the theoretical results of Negri et al. [14].

Correspondence to: P.H.M. van Loosdrecht, Research Institute of Materials, University of Nijmegen, Toernooiveld, 6525 ED Nijmegen, The Netherlands.

[#1] Available upon request ("buckybib", Department of Chemistry, Rice University, P.O. Box 1892, Houston, Texas 77251, USA).

2. Selection rules

The high symmetry (I_h) of the C_{60} molecule has a large influence on its vibrational properties. Although C_{60} has 174 internal degrees of freedom the

icosahedral symmetry reduces this large number to only 46 distinct vibrational modes, the group theoretical classification of which is given by $\Gamma_{C_{60}}^{mol} = 2A_g + 3F_{1g} + 4F_{2g} + 6G_g + 8H_g + A_u + 4F_{1u} + 5F_{2u} + 6G_u + 7H_u$. Experimentally, the number of observable modes is further reduced by selection rules. The strongest reduction occurs for infrared scattering, where only the $4F_{1u}$ modes are active. For Raman scattering, one expects the $2A_g$ and $8H_g$ modes to be active. The most complete picture can be obtained from inelastic neutron scattering, which has no selection rules at all. These differences in selection rules are very useful in the classification of the vibrational modes of the C_{60} molecule [15].

The vibrational modes and selection rules described above apply only to the free molecule. In the solid state the crystal field influences the vibrational properties as well as the selection rules. A distinction can be made between internal and external modes: the internal modes correspond to the molecular modes of vibration whereas the external modes are the translational and librational vibrations of the molecules as a whole. Because of the rather weak van der Waals bonding between the molecules in solid C_{60}, one expects that the frequencies of the internal modes are only slightly influenced, yielding small shifts and splittings of these modes. The crystal field effectively lowers the symmetry of the molecules, and therefore some of the molecular inactive modes will become active in the solid state.

The room-temperature structure of solid C_{60} is fcc (T_h^3) [16] with four equivalent molecules per conventional unit cell. This is possible because, due to the nearly complete rotational freedom, the molecules can be considered to be perfect spheres. At $T \approx 255$ K, the rotational motion of the molecules slows down critically and the crystal structure changes due to the faceted icosahedral nature of C_{60}. The low-temperature structure of C_{60} is usually considered to be sc (T_h^6) [5], with four orientationally inequivalent molecules per primitive cell. Recently, van Tendeloo et al. [12] found evidence for a superstructure below 100 K, pointing to a $2a_0$-fcc crystal structure with spacegroup T_h^4 for the low-temperature phase. In this structure the C_{60} molecules are rotated by an angle ϕ around the $\langle 111 \rangle$ directions, just as in the sc phase. In contrast to the sc structure, however, two groups of molecules can be distinguished in the $2a_0$-fcc structure, differing in rotation angle ϕ by 60° [17]. The presence of this superstructure has been unambiguously confirmed in triplet state EPR measurements on C_{60} single crystals [9]. It is likely that the phase transition from the fcc to the $2a_0$-fcc phase occurs in two steps. At the 255 K transition the rotational disorder freezes, leaving the possibility of rotational excitations involving jumps between the almost equivalent orientations of the two groups of molecules [6,7]. This makes the two groups equivalent, and the structure is therefore simple cubic. At low temperatures [17,18] these rotational jumps also freeze, leading to the low-temperature $2a_0$-fcc structure.

In both the low- and high-temperature phases the inversion symmetry on the molecular sites is retained, which ensures a persistence of the complementarity of infrared and Raman spectroscopy. The symmetry splittings of the modes in the fcc, $2a_0$-fcc and sc structures can be determined using factor group analysis. For the $2a_0$-fcc and sc phase, this can be accomplished by taking the site symmetry S_6 into account. The results of this exercise are shown in table 1, which indicates the correlation between the molecular modes and the solid state modes in the fcc, $2a_0$-fcc and sc phases. The resulting number of modes derived from table 1, as well as the number of external modes are shown in table 2 together with their activity in Raman and infrared spectroscopy. A detailed discussion of the group theoretical aspects of the vibrational properties in the fcc and sc phase has been given by Dresselhaus et al. [19]. Instead of just the ten Raman active molecular modes, all gerade modes are expected to be active in solid C_{60} and one expects to observe 23 groups of modes in Raman

Table 1
Correlations between gerade modes of C_{60} for the free molecule (I_h) and the molecule in the fcc (T_h^3), $2a_0$-fcc (T_h^4) and sc (T_h^6) structures. The correlations for the ungerade modes are equivalent

I_h T_h^3	$T_h^4(2a_0)$	T_h^6
$A_g \rightarrow A_g$	$2A_g + 2F_g$	$A_g + F_g$
$F_{1g} \rightarrow F_g$	$2A_g + 2E_g + 6F_g$	$A_g + E_g + 3F_g$
$F_{2g} \rightarrow F_g$	$2A_g + 2E_g + 6F_g$	$A_g + E_g + 3F_g$
$G_g \rightarrow A_g + F_g$	$4A_g + 2E_g + 8F_g$	$2A_g + E_g + 4F_g$
$H_g \rightarrow E_g + F_g$	$2A_g + 4E_g + 10F_g$	$A_g + 2E_g + 5F_g$

Table 2
The number of internal (n_i) and external (n_e) vibrational modes in the fcc (T_h^3), $2a_0$-fcc (T_h^4) and sc (T_h^6) structures of solid C_{60}. The external modes have been labeled r, t and a for optical rotational, optical translational and acoustic, respectively. The first column gives the irreducible representation of the T_h point symmetry group of the cubic structures. The second column gives the activity in infra-red (IR) and Raman ($\parallel$R and $\perp$R for the scattered light respectively parallel and perpendicular to the excitation light) experiments. The total number of modes is given in the last row, with in parentheses the total number of Raman active modes

T_h	Act.	T_h^3		$T_h^4(2a_0)$		T_h^6	
		n_i	n_e	n_i	n_e	n_i	n_e
A_g	$\parallel$R	8	–	58	2^r	29	1^r
E_g	$\parallel$R	8	–	58	2^r	29	1^r
F_g	$\perp$R	21	1^r	174	6^r	87	3^r
A_u	–	7	–	60	2^t	30	1^t
E_u	–	7	–	58	2^t	29	1^t
F_u	IR	22	1^a	186	5^t, 1^a	93	2^t, 1^a
n_{total}		73(37)	2(1)	594(290)	20(10)	297(145)	10(5)

spectra. Since in the high-temperature phase the molecules rotate almost freely and are held together by the relatively weak van der Waals interaction, the electronic structure of the C_{60} molecules hardly changes as compared to the free molecule and the splittings are expected to be relatively small. In the same vein, the additional modes induced by the symmetry reduction are expected to be weak. In the low-temperature phase a perturbation of the electronic structure of the C_{60} molecules can be expected since the electrostatic interaction between the electron rich and electron poor parts of the molecules is no longer negligible [20].

The numerical differences in the selection rules for Raman scattering in the $2a_0$-fcc and sc structures can theoretically be used to investigate whether or not the sc structure exists as an intermediate phase between the $2a_0$-fcc and fcc phases. Because the expected frequency differences due to the superstructure are, however, very small it seems doubtfully that these differences can be observed experimentally. It is more likely that the distinction between the sc and the $2a_0$-fcc phase is observable in the number of IR active external translational, or Raman active external rotational modes.

3. Raman spectra of single crystal C_{60}

The production of the high-purity C_{60} single crystals used in this study has been described in detail elsewhere [21]. The vapor growth method used ensures a high crystal quality, as well as a further purification of the chromatographically purified starting material. The absence of impurities such as residual solvents, oxygen or other fullerenes is extremely important because they strongly influence the structural and dynamical properties of solid C_{60}. The crystal quality, already indicated by the morphology revealing only {100} and {111} faces, has been checked on crystals obtained from the same growth batch. X-ray diffraction revealed a fcc structure at room temperature with no indications for any other phase [22]. High-resolution electron microscopy [23] confirmed the pure fcc phase and also revealed some structural defects, common to this kind of cubic structures.

The crystals used in the experiments are mounted in a flow cryostat (temperature stabilization better than 0.1 K, absolute temperature ± 2 K), which was evacuated to 5×10^{-6} mbar immediately after (within a few minutes) they are either removed from their vacuum-kept quartz growth tubes, or cleaved in air. This procedure prevents the degradation of the samples that occurs when the crystals are kept in air and ensures a clean surface. This is of vital importance since the presence of oxygen degrades the samples, leading to changes in the electronic and vibrational properties [24]. Raman experiments have been performed in a backscattering geometry using a DILOR multichannel spectrometer (spectral slit width 3.5 cm^{-1} at 514 nm, and 1.5 cm^{-1} at 740 nm),

with either an argon ion laser (514 nm, $d \approx 30$ μm spot) as excitation source, or a Ti:sapphire laser (740 nm). C_{60} is easily excited into a triplet state under the influence of 514 nm radiation. Since the interest of the present work is the ground state vibrational properties of C_{60}, the irradiance has been kept below 5 W/cm^2. It has been shown [24] that at least in the low-temperature phase the population of the triplet states is negligible at these irradiances.

Fig. 1 shows the unpolarized Raman spectra of C_{60} as recorded in the high- (280 K, spectrum 1a) and the low-temperature phase (40 K, spectrum 1b) under 514 nm excitation. A large number of internal modes is observed in both phases (49 in the low-temperature phase and 21 in the high-temperature phase). Polarized Raman experiments at 100 K yielded an intensity ratio $I_\perp/I_\parallel$ of 0.3–0.9 for most of the peaks, and ≈ 0.02 for the two A_g modes. These modes correspond to an in-phase (496 cm^{-1}) and out-of-phase (1468 cm^{-1}) dilatory vibration of the hexagonal and pentagonal rings of the molecule. The spectra have been fitted to Lorentzian shaped peaks, which gave a satisfactory result. The fitted mode frequencies (ω_0), full width at half maximum (γ) and relative intensities (I) are tabulated for both phases in the first six columns of table 3.

Also shown in fig. 1 is the low-temperature (40 K) spectrum of C_{60} recorded using 740 nm, 150 W/cm^2 excitation (spectrum 1c). This spectrum has been corrected for the wavelength dependence of the detector response, and a blank excitation source spectrum has been subtracted. The peak frequencies, linewidths and relative peak intensities are listed in table 4. It should be noted that the penetration depth for 514 nm radiation in C_{60} is approximately 3 μm. For 740 nm, the penetration depth is orders of magnitude larger. The 150 W/cm^2 used for the 740 nm spectrum can therefore be considered as a low-irradiance excitation. The 740 nm and 514 nm spectra show comparable absolute intensities, despite the higher irradiance and the larger penetration depth for 740 nm excitation. This evidently reflects the resonance effects in the 514 nm spectra.

4. Interpretation of the spectra

The 514 nm spectra depicted in fig. 1 (spectra 1a and 1b) clearly show Raman activity in crystalline C_{60} of modes which are inactive for the free molecule . Moreover, a large number of splittings can be observed, especially in the low-temperature spectrum. Details of the spectra, revealing these splittings have been published previously [10]. Both re-

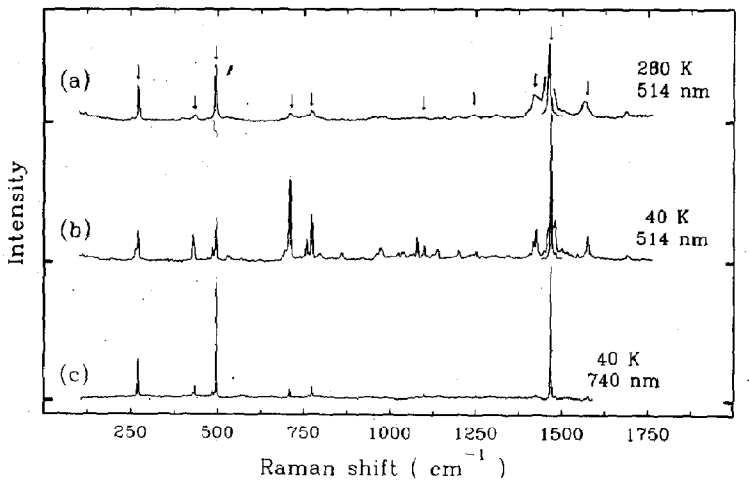

Fig. 1. Unpolarized Raman spectra of single crystal C_{60} for (a) $T \approx 280$ K, $\lambda_{laser} = 514$ nm, (b) $T = 40$ K, $\lambda_{laser} = 514$ nm, and (c) $T \approx 40$ K, $\lambda_{laser} = 740$ nm. The modes which are Raman active for the free molecule are denoted by an arrow in spectrum (a). The strong out-of-phase ring mode at ≈ 1468 cm^{-1} has been scaled down by a factor of 5 in spectra (a) and (b). The 740 nm spectrum (c) has been corrected for the detector response and a blank excitation source spectrum has been subtracted.

Table 3
Vibrational modes of C_{60}. In the first six columns the frequency ω_0, linewidth γ and relative intensity I of the observed Raman modes are given for respectively the fcc (280 K) and the $2a_0$-fcc (40 K) phase. The column labeled IN/IR/CS_2 lists the frequencies observed by inelastic neutron scattering at 25 K [13], room-temperature infrared spectroscopy [2] (marked with *), and by Raman spectroscopy for C_{60} dissolved in CS_2 at room temperature (this work, marked with †). In the last column the tentative assignments of the modes are given. The column labeled ref. [14] gives the calculated vibrational frequencies of Negri et al.

280 K (fcc)			40 K ($2a_0$-fcc)			IN/IR/CS_2	Ref. [14]	Assignment
ω_0 (cm^{-1})	γ (cm^{-1})	I (au)	ω_0 (cm^{-1})	γ (cm^{-1})	I (au)	ω_0 (cm^{-1})	ω_0 (cm^{-1})	
			57					
			80			80		
			108			102		lattice
						137		
			262	4	1.2	264 †	258	
			266	5	2.0			H_g
272	4	9.4	272	3	4.4	271		
						344	358	G_u
						355	531	H_u
						404	350	F_{2u}
						404	403	G_u or H_u
			428	4	4.4	425 †	440	
432	11	2.4	433	4	1.8	432		H_g
			485	4	2.2	488	476	G_g
			492	4	1.1	491 †	513	
494	5	8.3	496	3	5.1	488		A_g
						526, 527 *	544	F_{1u}
526	21	1.7	527	5	0.7		597	
			533	16	3.4	536		F_{1g}
						563, 577 *	637	F_{1u}
			567	8	1.1		614	
			579	6	0.4	576		G_g
			600	7	0.4		637	F_{2g}
						673	690	F_{2u}
			696	14	5.7		691	
708	12	2.7	709	4	14.2	715		H_g
724	7	0.4	738	16	2.5			
759	70	10.4	757	6	5.0		770	
			764	8	0.1			G_g
772	8	1.6	772	4	8.3	765	801	
			796	14	3.9			H_g
						813	999	F_{2u}
			860	9	2.7	840	834	F_{2g}
						890	1212	F_{2u}
			914	3	0.3		890	
			922	7	0.9			F_{2g}
962	45	8.1	959	8	1.5			
			972	13	6.7	971		
			1022	8	2.0	971	975	
1036	16	0.7	1038	12	4.1	1044		F_{1g}
1080	24	4.2	1079	4	3.3	1100 †	1154	
			1099	7	3.7	1089		H_g
			1110	4	0.4			
			1126	15	2.6	1122	1158	
1154	22	1.7	1138	8	3.7			G_g
						1183*	1241	F_{1u}

Table 3
Continued

280 K (fcc)			40 K ($2a_0$-fcc)			IN/IR/CS_2	Ref. [14]	Assignment
ω_0 (cm^{-1})	γ (cm^{-1})	I (au)	ω_0 (cm^{-1})	γ (cm^{-1})	I (au)	ω_0 (cm^{-1})	ω_0 (cm^{-1})	
1193	28	1.4	1200	7	2.1	1247 †	1265	
1243	46	2.9	1244	20	1.2	1217		H_g
			1252	4	0.6			
1307	37	2.3	1345	11	1.5	1327	1389	F_{1g}
						1428 *	1437	F_{1u}
1422	25	15.2	1406	8	0.1	1426 †	1465	
			1417	5	2.6			H_g
			1425	5	5.9			
1463	8	100	1468	4	100	1448, 1468 †	1442	A_g
1478	6	1.7	1480	7	6.6		1450	G_g
			1499	12	4.4			
1506	16	1.1	1514	14	3.3		1470	F_{2g}
			1528	10	1.5	1520		
			1544	6	1.3	1571 †	1644	
1566	20	10.5	1566	16	2.4	1563		H_g
			1575	6	5.4			
						1603		F_{2u}
1687	13	2.6	1687	3	0.6	1702	1585	G_g
			1694	9	1.4			

Table 4
Peak frequencies ω_0, linewidth γ and relative peak intensities I of the Raman active modes in C_{60} for 740 nm excitation. Only the clearest modes are given

ω_0 (cm^{-1})	γ (cm^{-1})	I (au)	ω_0 (cm^{-1})	γ (cm^{-1})	I (au)
266	1.5	11	1079	2	1
272	1.5	30	1100	2	3
274	2	7	1244	2	2
429	4	3	1251	3	2
434	1.5	10	1425	2	2
484	3.5	4	1468	2	100
496	1	84	1481	3	2
708	2	7	1576	3	4
773	2	8			

sults are consistent with the selection rules derived in section 1. In particular, all gerade molecular modes are observed in the low-temperature spectrum. Also the 740 nm spectrum (spectrum 1c and table 4) shows some new lines and splittings, although less prominent than in the 514 nm spectra. Except for one mode at 274 cm^{-1}, all peaks observed in the 740 nm spectra are also found in the spectra recorded using 514 nm excitation. The presence of this mode in the 740 nm spectrum is probably caused by the improved spectral resolution (1.5 cm^{-1}) of this spectrum.

There are two possible causes for the difference in the number of observed peaks in the 514 and 740 nm spectra. In the first place weak peaks are difficult to detect in the red part of the spectrum because of the reduced detector efficiency, and also due to the presence of broad spectral features of the Ti:sapphire laser. Secondly, resonance effects play an important role in the 514 nm spectrum [25]. Modes which are only weakly active using 740 nm excitation are strongly enhanced in the 514 nm spectrum. Even non-resonant first-order inactive modes can become active near the resonance, although normally these modes are only observed very close to the actual resonance. It is assumed that all observed peaks in the 514 nm spectrum, listed in table 3, result from resonance-enhanced first-order Raman processes. The relative intensities of the Raman bands presented in figs. 1a and 1b are also strongly influenced by the (pre)resonant enhancement of electronic nature. This is evident from a comparison of these spectra

to the spectrum presented in fig. 1c, and to the FT-Raman spectra obtained by Chase and Fagan [26] recorded using 1.064 μm excitation. The non-resonant data show comparable intensities for the two A_g modes and the H_g squashing mode, whereas near the resonance the out-of-phase ring mode is found to be a factor of five stronger. Moreover, the two H_g modes at 1100 and 1250 cm^{-1}, which have a pronounced presence in the 1.064 μm spectra [26], are of very low intensity in the spectra of figs. 1a and 1b.

Polarized 514 nm Raman experiments at $T=100$ K show that the A_g modes are weakly active in the perpendicular scattering geometry. This is consistent with the $2a_0$-fcc structure for the low-temperature phase. In the fcc phase, the A_g modes are also found to be active in the perpendicular scattering geometry, indicating a violation of the selection rules in this case. This may be induced by defect structures in the fcc phase. There are several differences between the spectra of the low- and high-temperature phases (figs. 1a and 1b). The low-temperature spectra reveal newly activated modes and splittings of modes already active at high temperatures, reflecting the reduced symmetry in the $2a_0$-fcc phase. In general the frequencies of the modes in the low-temperature phase are shifted towards higher frequencies, accompanied by a decrease of the linewidths. Also changes in the intensities have been observed. The absolute intensities are generally found to be a factor of 3–4 stronger in the $2a_0$-fcc phase compared to those in the fcc phase. In addition to this, some of the relative intensities are drastically changed in the low-temperature phase, for instance the H_g modes in the 700–800 cm^{-1} region double in relative intensity compared to the fcc phase. The above described differences are partly due to the critical decrease of the rotational freedom in the low-temperature phase [10], partly to the changes in the electronic structure [20], i.e. in the resonance effects in the $2a_0$-fcc phase, and partly to the presence of triplet state excited C_{60}^* in the fcc phase. The softening associated with the presence of C_{60}^* [24] is illustrated in fig. 2, which shows the irradiance dependence of the frequency of the out-of-phase ring mode. For low irradiances (<10 W/cm^2) this mode softens reversibly, i.e. if the power density is decreased, the mode hardens again. For irradiances exceeding 10 W/cm^2 the spectra change irreversibly, indicating a "photo-transformation"

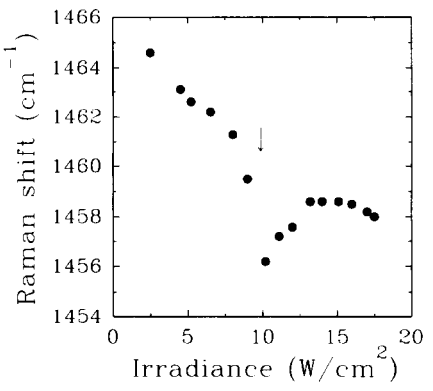

Fig. 2. Irradiance dependence of the frequency of the out-of-phase mode in single crystal C_{60}. The arrow indicates a "photo-transformation" of C_{60}.

[27] of C_{60}. The character of this transformation is still unclear, but, in view of the relatively large frequency shift, it seems likely that it involves a molecular transformation rather than structural changes of the crystal lattice. Extrapolating from fig. 2, the ground-state frequency of the out-of-phase mode is estimated to be 1466 cm^{-1}, consistent with the 300 K results obtained with 740 nm excitation (not shown here).

Apart from the Raman data of this work, table 3 shows the infrared data of Krätschmer et al. [2], and the neutron scattering data of Coulombeau et al. [13], as well as the frequencies obtained from Raman spectra (514 nm) of C_{60} dissolved in CS_2. By combining the data of the different experimental methods, and the theoretical results obtained by Negri et al. [14] (see table 3), one can come to an assignment of the observed peaks to the various symmetry modes of the free C_{60} molecule. This is done in the last column of table 3. It is clear from table 3 that all gerade modes are indeed observed in the Raman spectra. The frequencies of the observed experimental modes agree very well with the results of ref. [14], in which the authors performed their calculations at a time when no experimental data were available. Recently, Negri et al. [15] showed that their results compare very well to other experimental data not discussed here, including Raman [28], inelastic neutron scattering [29], and high-resolution energy-loss spectroscopy [30] results. A further improvement and extension of the assignment to the sym-

metry modes can be expected when low-temperature infrared data on single crystal C_{60} becomes available, data that can reveal most of the ungerade modes (see tables 1 and 2).

In the low-frequency part of the fcc spectra, a broadening of the Rayleigh wing is observed, which extends to $\approx 150\ cm^{-1}$. Part of the intensity here can be explained by the, to some extend, disordered surface of C_{60}, which induces diffuse scattering of the incident laser beam. However, one should consider that the rotational excitations of C_{60} are also a source of low-frequency scattering, and may be responsible for part of the intensity in this region. At low temperatures, the broadening of the Rayleigh wing is found to be strongly reduced. Furthermore, often some additional structure is observed at 56, 80 and 108 cm^{-1}. This structure is not observed in all spectra and the presence depends on the spot position on the crystal. Therefore, it seems feasible that it is induced by the presence of impurities or by defects in the crystal structure. This is in line with the observed violation of the selection rules for the A_g modes. Distinct low-frequency peaks have also been observed in inelastic neutron scattering experiments [13], confirming that they originate from external motions of C_{60}. In Raman scattering only the external rotational modes are expected to be active. The relatively high frequencies, however, indicate that these peaks cannot be of rotational origin and it is more likely that the structure results from activated translational modes. Using the inter-molecular potential derived by Girifalco [31], the frequencies of the external vibrational modes, which are proportional to $\sqrt{M^{-1}\partial^2 V(r)/\partial r^2}$, can be estimated to lie in the range of 25–85 cm^{-1}. Since the Girifalco potential neglects the contribution of the electrostatic interaction [20], this estimate can be considered to give a lower boundary for the translational modes. Coulombeau et al. [13] explained the discrepancy between theoretical predictions [32] and their neutron scattering results by assuming a rather strong temperature dependence of these modes. The low-frequency features reported here do not show a strong temperature dependence. Far infrared experiments might give some more insight in the low-frequency vibrational properties of C_{60}.

5. Conclusion

The vibrational properties of solid C_{60} in the low- and high-temperature phase have been studied using low irradiance, 514 nm Raman spectroscopy. The wavelength used has the advantage that resonance enhancements reveal Raman active modes which cannot be observed in non-resonant Raman spectroscopy. It has been shown that, within the experimental accuracy, the spectra of the different crystal phases are in agreement with the selection rules as derived in section 2, and a full symmetry assignment of the observed peaks has been proposed. Spectra recorded using 740 nm excitation show that the differences in the Raman spectra recorded at 514 nm for the high- and low-temperature phase are partly due to the rotational ordering, to changes in the resonance Raman cross sections, and to the presence of triplet state excited C_{60}^* in the fcc phase.

Acknowledgement

This work was financially supported by the Dutch Foundation for Fundamental Research of Matter (FOM).

References

[1] H.W. Kroto, J.R. Heath, S.C. O'Brien, R.F. Curl and R.E. Smalley, Nature 318 (1985) 162.
[2] W. Krätschmer, L.D. Lamb, K. Fostiropoulos and D.R. Huffman, Nature 347 (1991) 354.
[3] R.E. Smalley, The almost (but never quite) complete buckminsterfullerene bibliography.
[4] A.F. Hebard, M.J. Rosseinsky, R.C. Haddon, D.W. Murphy, S.H. Glarum, T.T.M. Palstra, A.P. Ramirez and A.R. Kortan, Nature 350 (1991) 600.
[5] P.A. Heiney, J.E. Fisher, A.R. McGhie, W.J. Romanow, A.M. Denenstein, J.P. McCauley Jr., A.B. Smith III and D.E. Cox, Phys. Rev. Letters 66 (1991) 2911;
R. Sachidanandam and A.B. Harris, Phys. Rev. Letters 67 (1991) 1467.
[6] R. Tycko, G. Dabbagh, R.M. Fleming, R.C. Haddom, A.V. Makhija and S.M. Zahurak, Phys. Rev. Letters 67 (1991) 1886.
[7] R.D. Johnson, C.S. Yannoni, H.C. Dorn, J.R. Salem and D.S. Bethune, Science 255 (1991) 1235.
[8] K. Sinha, J. Menéndez, R.C. Hanson, G.B. Adams, J.B. Page, O.F. Sankey, L.D. Lamb and D.R. Huffman, Chem. Phys. Letters 186 (1991) 287.

[9] E.J.J. Groenen, O.G. Poluektov, M. Matsushita, J. Schmidt, J.H. van der Waals and G. Meijer, Chem. Phys. Letters 197 (1992) 314.
[10] P.H.M. van Loosdrecht, P.J.M. van Bentum and G. Meijer, Phys. Letters 68 (1992) 1176.
[11] S.J. Duclos, R.C. Haddon, S. Glarum, A.F. Hebbard and K.B. Lyons, Science 254 (1991) 1625.
[12] G. van Tendeloo, S. Amelinckx, M.A. Verheijen, P.H.M. van Loosdrecht and G. Meijer, Phys. Rev. Letters, in press.
[13] C. Coulombeau, H. Jobic, P. Bernier, C. Fabre, D. Schütz and A. Rassat, J. Phys. Chem. 96 (1992) 22.
[14] F. Negri, G. Orlandi and F. Zerbetto, Chem. Phys. Letters 144 (1988) 31.
[15] F. Negri, G. Orlandi and F. Zerbetto, Chem. Phys. Letters 190 (1992) 174.
[16] R.M. Fleming, A.P. Ramirez, M.J. Rosseinsky, D.W. Murphy, R.C. Haddon, S.M. Zahurak and A.V. Makhija, Nature 352 (1991) 787.
[17] W.I.F. David, R.N. Ibberson, T.J.S. Dennis, J.P. Hare and K. Prassides, Europhys. Letters 18 (1992) 219.
[18] X.D. Shi, A.R. Kortan, J.M. Williams, A.M. Kini, B.M. Savall and P.M. Chaikin, Phys. Rev. Letters 68 (1992) 827.
[19] G. Dresselhaus, M.S. Dresselhaus and P.C. Eklund, Phys. Rev. B 45 (1992) 6923.
[20] M. Sprik, A. Cheng and M.L. Klein, J. Phys. Chem. 96 (1992) 2027.
[21] M.A. Verheijen, H. Meekes, G. Meijer, E. Raas and P. Bennema, Chem. Phys. Letters 191 (1992) 339.
[22] J. de Boer, private communication.
[23] G. van Tendeloo, C. van Heurck, J. van Landuyt, S. Amelinckx, M.A. Verheijen, P.H.M. van Loosdrecht and G. Meijer, J. Phys. Chem, in press.
[24] P.H.M. van Loosdrecht, P.J.M. van Bentum, G. Meijer, Europhys. Letters, submitted for publication.
[25] M. Matus, H. Kuzmany and W. Krätschmer, Solid State Commun. 80 (1991) 839.
[26] B. Chase and P.J. Fagan, J. Am. Chem. Soc. 114 (1992) 2252.
[27] P. Zhou, A.M. Rao, K.-A. Wang, J.D. Roberson, C. Eloi, M.S. Meier, S.L. Ren, X.X. Bi and P.C. Eklund, Applied Phys. Letters 60 (1992) 287.
[28] D.S. Bethune, G. Meijer, W.C. Tang, H.J. Rosen, W.G. Golden, H. Seki, C.A. Brown and M.S. de Vries, Chem. Phys. Letters 179 (1991) 181.
[29] K. Prassides, T.J.S. Dennis, J.P. Hare, J. Thomkinson, H.W. Kroto, R. Taylor and D.R.M. Walton, Chem. Phys. Letters 187 (1991) 455;
R.L. Cappelletti, J.D.R. Copley, W.A. Kamitakahara, F. Li, J.S. Lannin and D. Ramage, Phys. Rev. Letters 66 (1991) 3261.
[30] G. Gensterblum, J.J. Pireaux, P.A. Thiry, R. Caudano, Ph. Lambin, A.A. Lucas and K. Krätschmer, Phys. Rev. Letters 67 (1991) 2171.
[31] L.A. Girifalco, J. Phys. Chem. 96 (1992) 858.
[32] A. Cheng and M.L. Klein, J. Phys. Chem. 95 (1991) 6750.